Assessment of blood-brain barrier disruption using dynamic contrast-enhanced MRI. A systematic review

NeuroImage: Clinical 6 (2014) 262–274

Contents lists available at ScienceDirect

NeuroImage: Clinical

journal homepage: www.elsevier.com/locate/ynicl

Assessment of blood–brain barrier disruption using dynamic contrast-enhanced MRI. A systematic review

Anna K. Heye[a], Ross D. Culling[b], Maria del C. Valdés Hernández[a], Michael J. Thrippleton[a], Joanna M. Wardlaw[a,*]

[a]Neuroimaging Sciences, University of Edinburgh, Edinburgh, UK
[b]College of Medicine and Veterinary Medicine, University of Edinburgh, Edinburgh, UK

ARTICLE INFO

Article history:
Received 18 July 2014
Received in revised form 4 September 2014
Accepted 5 September 2014
Available online 10 September 2014

Keywords:
Dynamic contrast-enhanced MRI
Permeability
Perfusion
Blood–brain barrier

ABSTRACT

There is increasing recognition of the importance of blood–brain barrier (BBB) disruption in aging, dementia, stroke and multiple sclerosis in addition to more commonly-studied pathologies such as tumors. Dynamic contrast-enhanced MRI (DCE-MRI) is a method for studying BBB disruption in vivo. We review pathologies studied, scanning protocols and data analysis procedures to determine the range of available methods and their suitability to different pathologies. We systematically review the existing literature up to February 2014, seeking studies that assessed BBB integrity using T1-weighted DCE-MRI techniques in animals and humans in normal or abnormal brain tissues. The literature search provided 70 studies that were eligible for inclusion, involving 417 animals and 1564 human subjects in total. The pathologies most studied are intracranial neoplasms and acute ischemic strokes. There are large variations in the type of DCE-MRI sequence, the imaging protocols and the contrast agents used. Moreover, studies use a variety of different methods for data analysis, mainly based on model-free measurements and on the Patlak and Tofts models. Consequently, estimated K^{Trans} values varied widely. In conclusion, DCE-MRI is shown to provide valuable information in a large variety of applications, ranging from common applications, such as grading of primary brain tumors, to more recent applications, such as assessment of subtle BBB dysfunction in Alzheimer's disease. Further research is required in order to establish consensus-based recommendations for data acquisition and analysis and, hence, improve inter-study comparability and promote wider use of DCE-MRI.

Contents

* Corresponding author at: Brain Research Imaging Centre, Neuroimaging Sciences, University of Edinburgh, Western General Hospital, Crewe Road, Edinburgh EH4 2XU, UK.
E-mail address: joanna.wardlaw@ed.ac.uk (J.M. Wardlaw).

http://dx.doi.org/10.1016/j.nicl.2014.09.002

1. Introduction

The blood–brain barrier (BBB) separates the parenchyma of the central nervous system from the blood. Quantitative information about the functional integrity of the BBB can be gained by performing dynamic contrast-enhanced MRI (DCE-MRI). DCE-MRI has proven valuable in the assessment of many brain pathologies that cause an opening of the BBB, such as tumors (Singh et al., 2007), multiple sclerosis (Jelescu et al., 2011) and acute ischemic strokes (Kassner et al., 2009). While these diseases show relatively large abnormalities in BBB functionality, there is also growing interest in the application of DCE-MRI to pathologies associated with more subtle and chronic BBB disruption, such as cerebral small vessel disease (Wardlaw et al., 2008; Wardlaw et al., 2009), diabetes (Starr et al., 2003) and Alzheimer's disease (Starr et al., 2009).

Although DCE-MRI has been widely used to study pathological changes in BBB functionality, studies differ in their MR imaging procedures and have been performed using a variety of different MRI sequences, contrast agents and time courses. Furthermore, there is no standard method for analyzing the data. Established analysis approaches include relatively simple non-model based methods (Topakian et al., 2010) as well as a range of pharmacokinetic models (Tofts, 1991). Several previous reviews have focused on specific applications such as oncology (Türkbey et al., 2010; Jain, 2013; Barnes et al., 2012) and on methodological aspects of DCE-MRI (Sourbron and Buckley, 2012, 2013); as far as we are aware, there are no reviews that cover the application of DCE-MRI in aging, microvascular disease or dementia. The aim of this work is to provide an overview of all applications and scanning protocols used in DCE-MRI of the brain by performing a systematic review of the literature. First, we describe the important components of the BBB and available permeability models, then review available data on BBB permeability imaging. Furthermore, we aim to identify the most commonly used methods for data analysis and provide an overview of the resulting parameter ranges.

2. Background

2.1. Blood–brain barrier functionality

The BBB is formed by endothelial cells that line brain capillaries and are sealed by tight junctions, which are unique to the brain microvasculature. The endothelium of the BBB interacts with several cellular and non-cellular elements, such as astrocytes, pericytes, microglial cells and basement membranes, that provide both functional support and structural support to the BBB (Abbott and Friedman, 2012; Obermeier et al., 2013). Together they form an interactive cellular complex, the 'neurovascular unit' (NVU). A schematic drawing of the NVU is shown in Fig. 1. The BBB regulates the passage of essential molecules such as glucose, while restricting the diffusion of potentially harmful substances.

Many brain pathologies are known to cause a disruption of the BBB. The mechanisms that cause BBB opening are many and differ between diseases. In meningitis, for example, damage to the BBB is initiated by extrinsic systemic factors, such as infections and autoimmune processes. Other diseases, including Alzheimer's disease and ischemic stroke, are thought to activate intrinsic cellular mechanisms secondary to the neuroinflammatory injury and other as yet unknown processes (Rosenberg, 2012). Several comprehensive reviews provide detailed information on the molecular biology of BBB disruption in disease (Abbott and Friedman, 2012; Obermeier et al., 2013; Rosenberg, 2012).

2.2. Measurement of blood–brain barrier disruption using DCE-MRI

Disruption of the BBB can enable the extravasation of low-molecular weight MRI contrast agents. This accumulation of contrast material in the extravascular extracellular space (EES) of affected tissues leads to increased longitudinal relaxation rate and, therefore, increased signal intensity in T1-weighted images. DCE-MRI exploits this T1 enhancement in order to detect and evaluate regions of BBB disruption. The DCE-MRI procedure typically consists of intravenous injection of contrast agent followed by the repeated acquisition of T1-weighted images (see Fig. 2), providing measurements of signal enhancement as a function of time. The enhancement kinetics can be used to extract quantitative or semi-quantitative information regarding BBB integrity.

MR signal changes caused by contrast agent extravasation are determined by several factors, including tissue perfusion and capillary permeability. In the brain, DCE-MRI is considered to be the standard MRI approach for assessing permeability, while dynamic susceptibility contrast MRI (DSC-MRI) is the method of choice for perfusion imaging (Sourbron and Buckley, 2013). However, it has been shown that DCE-MRI can combine perfusion and permeability measurements by using a sufficiently long acquisition time (to capture slow interstitial uptake) with high temporal resolution early on (to capture the first pass of the contrast bolus) (Li et al., 2000; Li et al., 2012; Sourbron et al., 2009; Larsson et al., 2009).

2.3. Analysis of DCE-MRI data

Different approaches have been used to analyze DCE-MRI data, ranging from relatively simple visual assessment of enhancement curves to more complex fitting to pharmacokinetic models. Heuristic analysis of the signal enhancement curves provides semi-quantitative measures

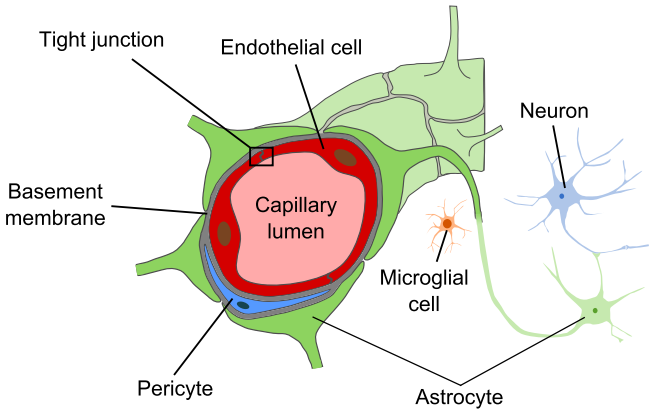

Fig. 1. Schematic drawing of the neurovascular unit. The BBB is formed by endothelial cells that line brain capillaries and are sealed by tight junctions. Astrocytes, pericytes, microglial cells and basement membranes interact with the endothelium of the BBB, providing functional and structural support.

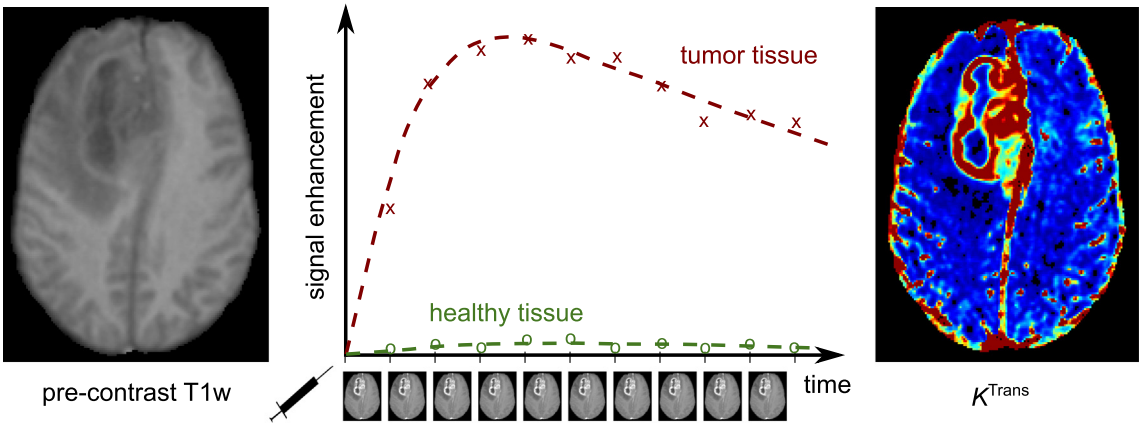

Fig. 2. Illustration of DCE-MRI in a patient with a glioma. The repeated acquisition of T1-weighted images after contrast agent injection allows the calculation of signal enhancement as a function of time (middle) when compared to the pre-contrast signal intensity (left). These curves can be used to calculate maps of quantitative pharmacokinetic parameters (e.g. K^{Trans}, right).

of BBB disruption, such as the area under the curve (AUC) and the time to maximum enhancement. Such measurements are easy to obtain but difficult to interpret (Budde et al., 2012). Quantitative analysis on the other hand aims to provide a link between the tissue signal enhancement and physiologically relevant parameters such as microvascular permeability, blood flow, blood volume fraction and interstitial volume fraction.

In order to relate the measured signal enhancement to the contrast agent concentration, an appropriate signal model is required. While early DCE-MRI studies assumed a linear relationship between signal enhancement and contrast uptake, it is well known that the signal enhancement is highly dependent on intrinsic tissue and acquisition parameters (Armitage et al., 2005; Armitage et al., 2011). Consequently, more complex approaches were developed in order to control for the effect of tissue characteristics such as the pre-contrast longitudinal relaxation time and the longitudinal and transverse relaxivities of the contrast agent (Armitage et al., 2005).

Pharmacokinetic modeling was first introduced for the analysis of DCE-MRI in the early 1990s by Brix et al. (1991), Larsson et al. (1990), and Tofts (1991), followed by a consensus paper on the notation (Tofts et al., 1999). Since then, improvement of the imaging techniques (e.g. higher temporal resolution and contrast-to-noise ratio) and a better understanding of the underlying physiology have promoted the development of several more complex pharmacokinetic models. Detailed reviews of tracer kinetic modelling approaches in DCE-MRI have been published by Sourbron and Buckley (2012, 2013). In the following, we will briefly describe a basic tissue model and the three most commonly used pharmacokinetic models in DCE-MRI.

Fig. 3A displays a general tissue model with exchange of contrast agent between blood plasma and the EES. Target parameters of pharmacokinetic modeling in DCE-MRI are the fractional plasma volume v_p, the fractional interstitial volume v_e, the plasma flow F_p and the permeability-surface area product PS, which measures the rate at which contrast agent particles leak out of the plasma and into the EES per unit tissue volume and plasma concentration. An important physiological parameter that is widely reported in DCE-MRI studies is the volume transfer constant K^{Trans}, which is the rate at which contrast agent is delivered to the EES per volume of tissue and contrast agent concentration in the arterial blood plasma. While the terms PS and K^{Trans} are sometimes used interchangeably in the literature, PS represents the clearance for contrast agent leaking from the capillary plasma into the EES, i.e. the flux of contrast agent across the BBB normalized to the tissue plasma concentration and tissue volume; in contrast, K^{Trans} (as implicitly defined by Tofts et al., 1999), is the contrast clearance normalized to the *arterial* plasma concentration and therefore depends on the plasma flow F_p supplying the capillaries in addition to PS (the mathematical form of this relationship is model-dependent). K^{Trans} is necessarily equal to the product of plasma flow F_p and the extraction fraction E (i.e. the fraction of contrast agent molecules that leak into the EES).

Most pharmacokinetic models require the arterial input function (AIF) to be known, which describes the tracer concentration in blood plasma over time. There are several strategies for determining the AIF (Calamante, 2013), including the use of a standard function (Weinmann et al., 1984), experimentally derived population-averaged AIFs (Parker et al., 2006) and simultaneous individual measurement of the AIF in a feeding vessel close to the tissue of interest (Sourbron et al., 2009).

The conventional Tofts model (Tofts, 1991) considers isodirectional flux of tracer between the two well-mixed blood plasma and EES compartments with the volume transfer constant K^{Trans}. The plasma compartment is assumed to have negligible volume ($v_p \approx 0$), which makes the classic Tofts model a one-compartment model for weakly vascularized tissues. This model is illustrated in Fig. 3B and characterized by the working Eq. (1):

$$C_t(t) = K^{Trans} \int_0^t C_p(\tau) \exp[-\frac{K^{Trans}(t-\tau)}{v_e}] d\tau, \quad (1)$$

where $C_p(t)$ is the AIF.

Tofts et al. extended their classic model by introducing the blood plasma as a second well-mixed and highly perfused compartment (Tofts et al., 1999; see Fig. 3C). In addition to the two parameters K^{Trans} and v_e, the model allows the fractional plasma volume v_p to be estimated and, hence, separates enhancement effects due to contrast leakage from those due to intravascular contrast:

$$C_t(t) = v_p C_p(t) + K^{Trans} \int_0^t C_p(\tau) \exp[-\frac{K^{Trans}(t-\tau)}{v_e}] d\tau. \quad (2)$$

If the model fits the data well with a non-negligible v_p value, then the tissue must be highly perfused ($F_p = \infty$) and the system is permeability-limited with $K^{Trans} = PS$ (Sourbron and Buckley, 2013).

Finally, the Patlak model also describes a highly perfused two-compartment tissue but considers unidirectional transport from the blood plasma into the EES (see Fig. 3D). The tracer concentration in tissue is given by

$$C_t(t) = v_p C_p(t) + K^{Trans} \int_0^t C_p(\tau) d\tau. \quad (3)$$

When first introducing this approach, Patlak and colleagues proposed a linear graphical analysis method, which is often used as it

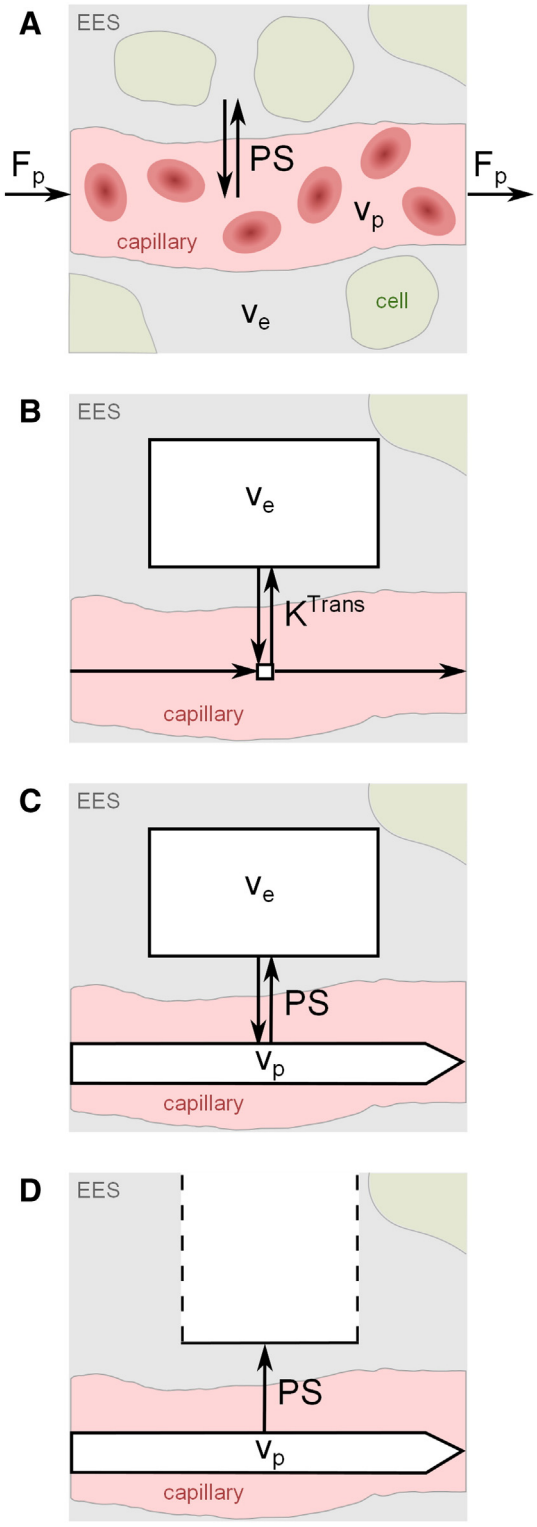

Fig. 3. Schematic illustrations of common pharmacokinetic models and target parameters. The exchange between the extravascular extracellular space (EES, volume fraction v_e) and capillary blood plasma (volume fraction v_p) is determined by the plasma flow F_p and the permeability-surface area product PS. (A) Generic tissue model. (B) Conventional Tofts model (with negligible blood volume and volume transfer constant K^{Trans}). (C) Modified Tofts model with non-negligible blood compartment. (D) Patlak model with non-negligible plasma compartment and one-way transport of contrast agent across the BBB. For the latter two models, it may be assumed that $K^{Trans} = PS$ for any solution fitting the data well with a non-negligible v_p.

permits simple and fast fitting. In this analysis, the ratio $C_t(t)/C_p(t)$ is regressed against $\int_0^t C_p(\tau)d\tau/C_p(t)$, yielding a straight line with slope K^{Trans} and y-intercept v_p.

3. Methods

3.1. Search strategy

The existing literature was systematically reviewed up to February 2014 by performing an electronic search in PubMed, EMBASE, MEDLINE and Web of Knowledge databases. Multiple combinations of the following search terms were used: 'permeability', 'brain', 'blood–brain barrier', 'MRI', 'dynamic', 'DCE-MRI' and 'contrast enhancement'. English as well as non-English literature was sought. The electronic search was supplemented by hand searching the reference lists of review papers.

One reviewer performed the primary literature search, removed duplicates and screened all papers' titles and abstracts in order to identify those relevant for full assessment. Before final inclusion or exclusion of studies, a second reviewer continued the search, read the full text of the selected articles, extracted the relevant data and performed the analysis. Disagreements between reviewers about inclusion or exclusion of papers were resolved through discussion with a third reviewer. The third, fourth and fifth reviewers complemented the search and assisted with the data analysis.

3.2. Eligibility criteria

We sought studies which assessed BBB integrity using dynamic contrast-enhanced MRI techniques. We included studies on humans and animals in all diseases known or thought to affect BBB function. Consequently, we excluded other applications of DCE-MRI such as breast or prostate cancer as well as publications that focus on theoretical aspects of image processing or modeling without testing them in a clinical setting (e.g. Gal et al., 2008). Furthermore, we accepted only primary research articles which were available as full-text, but checked review articles for additional primary references.

We excluded studies using non-dynamic MRI methods, DSC-MRI or non-MRI methods in order to decrease variability between studies, which is already considerable between DCE-MRI studies. The literature search yielded several papers that focused on therapeutic BBB disruption for novel anti-cancer drugs. Since these mainly addressed pharmaceutical or technical aspects of the disruption method on a molecular level, these studies were rejected. An excellent review on DCE-MRI in clinical trials of antivascular therapies can be found in O'Connor et al. (2012). However, we did include studies that focused on the clinical effect of treatment strategies and its link with BBB disruption if they provided baseline DCE-MRI parameters. Moreover, we rejected single case reports and articles in which substantial information about the MRI procedure or the data analysis was lacking.

3.3. Data extraction and analysis

One reviewer independently extracted the data from each included study and cross-checked information with preliminary extracted data. Disagreements were resolved by consensus. We noted the studied disease or pathology, sample size and subjects' ages (in the case of human studies). Moreover, we extracted details of the DCE-MRI protocol, noting scanner field strength, MRI sequence with repetition time (TR) and echo delay time (TE), field of view, matrix size, slice thickness, overall duration and temporal resolution. Extracted data also included the type and dose of contrast agent and the injection protocol. Furthermore, we noted whether post-processing techniques were applied prior to data analysis, the analysis method used and the tissues/locations analyzed. Where

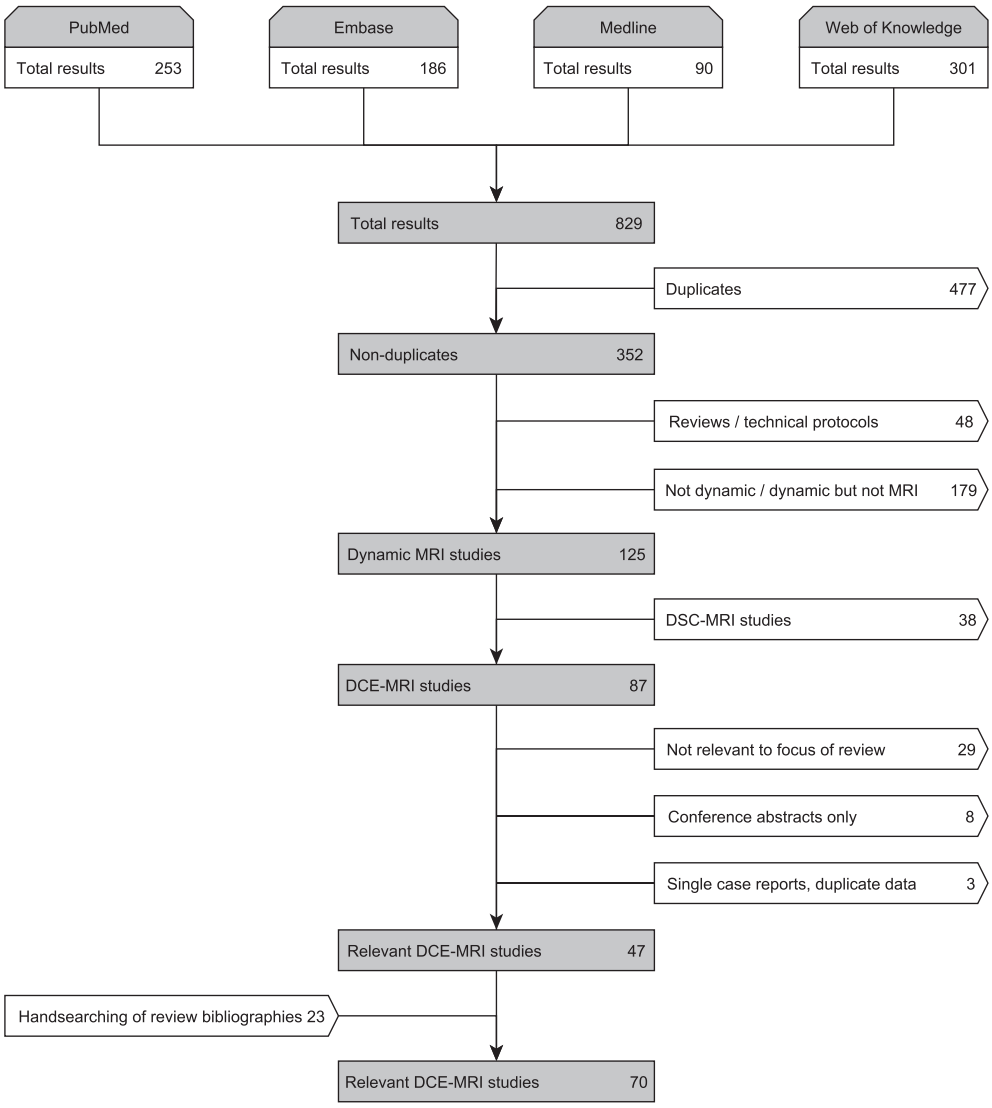

Fig. 4. Flow diagram summarizing the literature search and inclusion process.

given, quantitative measurements were extracted. We noted the main study purpose and the overall conclusion of the study.

In consequence of the large heterogeneity of included studies, quality assessment using standardized criteria as recommended in Guyatt et al. (2008) was difficult. However, we extracted limitations of the methodology where stated and whether any patients had been imaged but then excluded from further analysis, so as to assess the feasibility and applicability of the technique.

4. Results

4.1. Systematic literature search results

The electronic search yielded 829 results, 31 of which were in non-English languages. After removing duplicates, 352 publications were further analyzed for inclusion (see Fig. 4). After scanning abstracts and titles, we excluded studies using non-dynamic and non-MRI methods ($n = 179$). We also excluded review papers ($n = 46$), technical protocols ($n = 2$) and DSC-MRI studies ($n = 38$), leaving 87 articles for full-text assessment. At this stage, we identified 29 studies that were not relevant to the focus of this review. Moreover, we excluded conference abstracts that were not detailed enough for full data extraction and that had not subsequently been published in full ($n = 8$), single-case reports and publications with missing information on the imaging methodology ($n = 2$) and duplicate publications ($n = 1$). In addition to the resulting 47 relevant DCE-MRI studies, 23 relevant articles were identified by hand searching the bibliographies of review papers. Overall, the full literature search to February 2014 provided 70 DCE-MRI studies that were eligible for inclusion in this review, published between February 1990 (Kermode et al., 1990) and December 2013 (Cramer et al., 2014).

4.2. Subjects and sample sizes

Table 1 summarizes the main study sample characteristics and scanning protocols related to each pathology. Of the 70 included studies, 17 used animals (i.e. rodents (Budde et al., 2012; Abo-Ramadan et al., 2009; Ali et al., 2010; Durukan et al., 2009; Ewing et al., 2003; Ferrier et al., 2007; Nagaraja et al., 2010; Taheri et al., 2009; Hoff et al., 2012; Krueck et al., 1994; Li et al., 2010; Noseworthy and Bray, 2000; Quarles et al., 2012; Aryal et al., 2014; Brandt et al., 2008), apart from one study of beagle dogs (Su et al., 1998) and one of rabbits (Wei et al., 2011)). The sample size was not made available in one of these publications (Ewing et al., 2003). The mean sample size of the remaining animal studies was 25 animals, with a total number of 417 animals (including 19 healthy controls; 336/417 were rodents). The largest included study involved 113 rats (Abo-Ramadan et al., 2009), whereas

Table 1
Study sample characteristics and scanning protocols related to pathology. 'Mean age' displays the average of study mean ages for studies investigating the same pathology.

Pathology	Sample				Scanning protocol		References
	Subjects	Number of studies	Number of subjects	Mean age (years)	Median imaging duration (min)	Median temporal resolution (sec)	
Intracranial neoplasms	Humans	30	716	48.4	5.5	5.3	Singh et al. (2007); Li et al. (2000); Li et al. (2012); Sourbron et al. (2009); Larsson et al. (2009); Larsson et al. (1990); Haris et al. (2008a,c); Thompson et al. (2012); Miyati et al. (1997); Awasthi et al. (2012); Roberts et al. (2000); Bagher-Ebadian et al. (2012); Manuchehri et al. (2007); Cao et al. (2009); Cha et al. (2006); Chu et al. (2012); Harrer et al. (2004); Ludeman et al. (2002); Lüdemann et al. (2009); Lüdeman et al. (2000); Mills et al. (2009); Provenzale et al. (2006); Zhu et al. (2000); Ferl et al. (2010); Jia et al. (2013); Larsen et al. (2013); Wilkinson et al. (2006); Zhang et al. (2012); Larsson et al. (2013)
	Animals	8	140	—	15.0	11.5	Budde et al. (2012); Ali et al. (2010); Ferrier et al. (2007); Hoff et al. (2012); Krueck et al. (1994); Li et al. (2010); Quarles et al. (2012); Aryal et al. (2014)
Stroke / cerebrovascular disease	Humans	11	482	65.9	9.0	14.0	Kassner et al. (2009); Wardlaw et al. (2008); Wardlaw et al. (2009); Topakian et al. (2010); Armitage et al. (2011); Aksoy et al. (2013); Vidarsson et al. (2009); Kassner et al. (2005); Thornhill et al. (2010); Taheri et al. (2011a,b)
	Animals	5	154	—	25.0	150.0	Abo-Ramadan et al. (2009); Durukan et al. (2009); Ewing et al. (2003); Nagaraja et al. (2010); Taheri et al. (2009)
Multiple sclerosis	Humans	8	186	41.3	21.8	34.8	Jelescu et al. (2011); Larsson et al. (1990); Kermode et al. (1990); Cramer et al. (2014); Taheri et al. (2011b); Gaitán and Shea (2011); Shinohara et al. (2011); Ingrisch et al. (2012)
Pneumococcal meningitis	Animals	1	42	—	n/a	n/a	Brandt et al. (2008)
Zinc deficiency	Animals	1	36	—	36.0	240.0	Noseworthy and Bray (2000)
Neurocysticercosis	Humans	1	35	n/a	3.0	5.7	Gupta et al. (2012)
Traumatic head injuries	Animals	1	30	—	7.5	15.0	Wei et al. (2011)
Alzheimer's disease	Humans	1	30	73.7	34.4	229.0	Starr et al. (2009)
Multiple system atrophy	Humans	1	29	59.0	6.0	7.7	Song et al. (2011)
Infective brain lesions	Humans	1	26	26.6	2.8	5.3	Haris et al. (2008a)
Mild cognitive impairment	Humans	1	22	47.0	6.8	25.5	Wang et al. (2006)
Diabetes	Humans	1	20	68.2	90.0	900.0	Starr et al. (2003)
Brain tuberculomas	Humans	2	18	23.2	2.8	5.3	Singh et al. (2007); Haris et al. (2008b)
Normal aging	Animals	1	15	—	12.0	15.0	Su et al. (1998)

two studies used a sample size smaller than ten (Ferrier et al., 2007; Li et al., 2010).

The remaining 53 studies were in humans, including 1564 subjects in total (163 of which were healthy controls). The mean sample size for human studies was 27. Only one study involved more than 100 subjects (Haris et al., 2008a) and six studies were based on fewer than ten humans (Jelescu et al., 2011; Larsson et al., 1990; Kermode et al., 1990; Thompson et al., 2012).

Information regarding patient age was not provided in seven of the 53 studies (Li et al., 2000; Li et al., 2012; Sourbron et al., 2009; Larsson et al., 1990; Aksoy et al., 2013; Miyati et al., 1997; Awasthi et al., 2012). A further seven publications stated only the age range of the study subjects (Awasthi et al., 2012; Haris et al., 2008b; Roberts et al., 2000; Vidarsson et al., 2009; Bagher-Ebadian et al., 2012; Kassner et al., 2005; Manuchehri et al., 2007). Mean age as stated in the remaining 39 human studies was highly dependent on the studied pathology, ranging between 9 years (Thompson et al., 2012) (pediatric brain tumors) and 74 years (Wang et al., 2006) (mild cognitive impairment).

4.3. Pathologies studied

The majority of animal studies concerned intracranial neoplasms (Budde et al., 2012; Ali et al., 2010; Ferrier et al., 2007; Hoff et al., 2012; Krueck et al., 1994; Li et al., 2010; Quarles et al., 2012; Aryal et al., 2014) including a total of 140/417 animals. Five publications investigated changes in the BBB caused by induced focal cerebral ischemia in 154/417 animals overall (Abo-Ramadan et al., 2009; Durukan et al., 2009; Ewing et al., 2003; Nagaraja et al., 2010; Taheri et al., 2009). Moreover, one study each focused on the influence of pneumococcal meningitis (Brandt et al., 2008), normal aging (Su et al., 1998), zinc deficiency (Noseworthy and Bray, 2000) or traumatic head injuries (Wei et al., 2011) on the BBB.

The pathology most studied in humans was intracranial neoplasms (30 publications, 716/1564 subjects), including primary brain tumors and brain metastases (Li et al., 2012; Sourbron et al., 2009; Larsson et al., 2009; Larsson et al., 1990; Haris et al., 2008a,c; Thompson et al., 2012; Miyati et al., 1997; Awasthi et al., 2012; Roberts et al., 2000; Bagher-Ebadian et al., 2012; Manuchehri et al., 2007; Cao et al., 2009; Cha et al., 2006; Chu et al., 2012; Harrer et al., 2004; Ludemann et al., 2002; Lüdemann et al., 2009; Lüdemann et al., 2000; Mills et al., 2009; Provenzale et al., 2006; Zhu et al., 2000; Ferl et al., 2010; Jia et al., 2013; Larsen et al., 2013; Wilkinson et al., 2006; Zhang et al., 2012). Eleven studies investigated changes in BBB integrity caused by stroke and/or cerebrovascular disease (Kassner et al., 2009; Wardlaw et al., 2008; Wardlaw et al., 2009; Topakian et al., 2010; Armitage et al., 2011; Aksoy et al., 2013; Vidarsson et al., 2009; Kassner et al., 2005; Thornhill et al., 2010; Taheri et al., 2011a,b) with a total of 482/1564 subjects. Eight studies focused on multiple sclerosis (Jelescu et al., 2011; Larsson et al., 1990; Kermode et al., 1990; Cramer et al., 2014; Taheri et al., 2011b; Gaitán and Shea, 2011; Shinohara et al., 2011; Ingrisch et al., 2012) including a total of 186/1564 subjects. Other pathologies included Alzheimer's disease (Starr et al., 2009), mild cognitive impairment (Wang et al., 2006), brain tuberculomas (Singh et al., 2007; Haris et al., 2008b), infective brain lesions (Haris et al., 2008a), multiple system atrophy (Song et al., 2011), diabetes (Starr et al., 2003) and neurocysticercosis (Gupta et al., 2012).

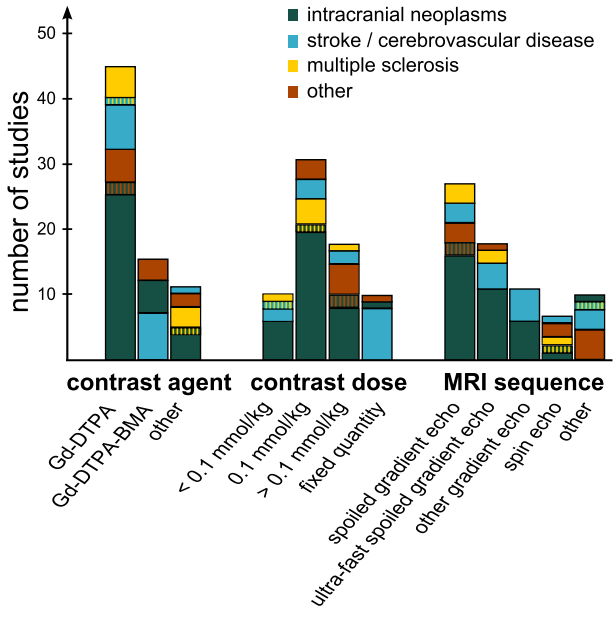

Fig. 5. Summary of contrast agents, contrast agent doses and MRI sequences. The bar height indicates the number of studies using a particular method, subdivided by pathology.

4.4. Blood–brain barrier changes in disease

Thirteen of the 70 included studies aimed to investigate the correlation between a particular disease and BBB dysfunction. For this purpose, BBB disruption was quantified in order to test for a significant difference between diseased subjects and healthy controls. Significant differences compared to control subjects or healthy tissue were found in eight studies, investigating acute ischemic stroke (Abo-Ramadan et al., 2009), pneumococcal meningitis (Brandt et al., 2008), brain metastases (Budde et al., 2012), multiple system atrophy (Song et al., 2011), type-II diabetes (Starr et al., 2003), vascular cognitive impairment (Taheri et al., 2011a), normal-appearing and lesion tissue in multiple sclerosis patients (Cramer et al., 2014; Taheri et al., 2011b), mild cognitive impairment (Taheri et al., 2011b), zinc deficiency (Noseworthy and Bray, 2000) and small vessel disease (Topakian et al., 2010). Moreover, Starr et al. observed differences in signal intensity profiles over time between Alzheimer's disease patients and controls (Starr et al., 2009). Increased BBB disruption without statistical significance was observed in patients with mild cognitive impairment (Wang et al., 2006). Su et al. showed a non-significant increase in BBB permeability with normal aging in beagle dogs (Su et al., 1998).

16 studies performed DCE-MRI in order to distinguish between different types or grades of pathology. Seven of those studies showed statistical significance that DCE-MRI derived parameters differentiate primary brain tumor types and grades (Roberts et al., 2000; Ludemann et al., 2002; Lüdemann et al., 2000; Mills et al., 2009; Zhu et al., 2000; Jia et al., 2013; Zhang et al., 2012). Furthermore, significant differences were found between infective vs. neoplastic brain lesions (Haris et al., 2008a), asymptomatic vs. symptomatic neurocysticercosis (Gupta et al., 2012), severe and moderate vs. mild traumatic brain injuries (Wei et al., 2011), and radiation necrosis vs. tumor recurrence (Larsen et al., 2013). Wardlaw et al. showed that post-contrast signal enhancement was higher in cerebrospinal fluid and white matter in lacunar (i.e. small vessel disease stroke) than in cortical (i.e. large artery atherothromboembolic stroke) patients (Wardlaw et al., 2008; Wardlaw et al., 2009). Kassner et al. found significantly different permeability scores between stroke patients who proceeded to hemorrhage and those who did not with and without thrombolytic therapy (Kassner et al., 2009; Kassner et al., 2005). Furthermore, Aksoy et al. (2013) reported significantly different DCE-MRI parameters for hemorrhagic strokes depending on their size and location.

4.5. Contrast agent and dose

The type and dose of contrast agents used in the included publications are summarized in Fig. 5. In most studies, the contrast agent used was Gd-DTPA (gadopentetate dimeglumine, 45/70 studies) or its variant Gd-DTPA-BMA (gadodiamide, 15/70 studies), given as an intravenous bolus injection. In 31 studies, this contrast agent was given in the standard dose of 0.1 mmol/kg body weight. However, delivered

doses ranged from 0.02 mmol/kg (Awasthi et al., 2012) to 0.5 mmol/kg (Ferrier et al., 2007). Ten studies delivered a fixed quantity of contrast agent, ranging between 7.5 mmol (Kassner et al., 2009; Vidarsson et al., 2009; Thornhill et al., 2010) and 20 mmol (Wardlaw et al., 2008; Wardlaw et al., 2009; Armitage et al., 2011) in humans. Single studies employed different gadolinium-based agents such as Gd-DOTA (gadoterate meglumine) (Li et al., 2000; Chu et al., 2012), gadobutrol (Gd-BT-DO3A) (Jelescu et al., 2011; Cramer et al., 2014; Wilkinson et al., 2006; Ingrisch et al., 2012; Song et al., 2011; Larsson et al., 2013), gadoteriol (Thompson et al., 2012) and albumin-labeled Gd-DTPA (Ali et al., 2010). We did not find any study that investigated the influence of different contrast agent types or concentrations, though Abo-Ramadan et al. state that different doses lead to an increase or decrease in signal-to-noise ratio (Abo-Ramadan et al., 2009).

4.6. Scanning techniques and field strength

The MRI pulse sequence types used are summarized in Fig. 5. The technique most frequently used was a spoiled gradient echo sequence (27 studies) and its ultra-fast variants (18 studies). Further protocols include 11 other gradient recalled echo sequences (Kassner et al., 2009; Larsson et al., 2009; Budde et al., 2012; Abo-Ramadan et al., 2009; Durukan et al., 2009; Hoff et al., 2012; Quarles et al., 2012; Kassner et al., 2005; Cao et al., 2009; Thornhill et al., 2010; Larsson et al., 2013), six spin-echo methods (Larsson et al., 1990; Kermode et al., 1990; Taheri et al., 2009; Krueck et al., 1994; Noseworthy and Bray, 2000; Su et al., 1998) and two unspecified T1-weighted imaging sequences (Starr et al., 2003; Song et al., 2011). Furthermore, two studies used a TOMROP (T-One by Multiple Read-Out Pulses) pulse sequence (Ewing et al., 2003; Nagaraja et al., 2010), two studies used T1 mapping of partial inversion recovery (TAPIR) (Taheri et al., 2011a,b), and one study each used a THRIVE (Wei et al., 2011), RF-FAST (Wang et al., 2006) and TWIST (Jia et al., 2013) sequence.

Four publications focused on introducing new scanning methods. A scanning procedure for combined and consecutive DSC- and DCE-MRI measurement was introduced by Miyati et al. (1997) and Thompson et al. (2012) respectively. Moreover, Jelescu et al. (2011) and Li et al. (2012) presented a dual-temporal resolution scanning method with high temporal resolution during the bolus first pass and high spatial resolution during the later phase.

The majority of human studies (35/53) were performed with a magnetic field strength of 1.5 T, while 16 studies used a 3 T scanner; one study each was performed using a 0.5 T (Kermode et al., 1990) and a 1.9 T scanner (Starr et al., 2003). A wider range of magnetic field strengths from 1.5 T (Krueck et al., 1994) to 11.75 T (Li et al., 2010) were found in animal studies, with the majority of studies using 4.7 or 7 T scanners. Two studies did not provide this information (Li et al., 2012; Wei et al., 2011).

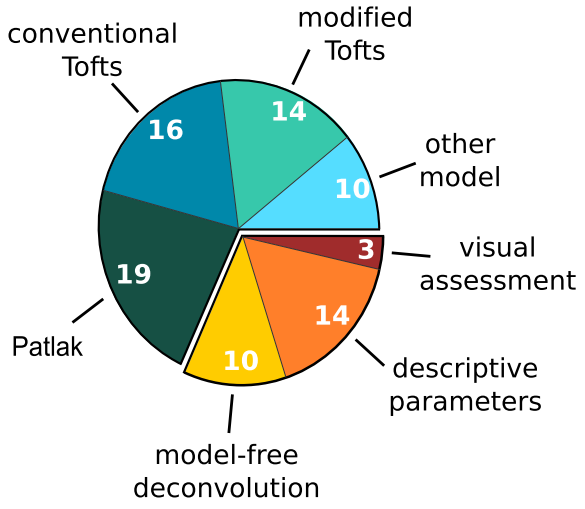

Fig. 6. Data analysis methods used in the included studies. Numbers indicate the count of studies using the particular method. (Note that some studies used more than one approach. Consequently, the numbers of studies do not add up to the 70 included studies.).

4.7. Duration and temporal resolution of DCE-MRI

The duration of data collection following contrast injection varied widely with values from 2.1 min (Miyati et al., 1997) to 155 min (Shinohara et al., 2011). The median DCE-MRI imaging durations (not stated in five publications (Larsson et al., 1990; Li et al., 2010; Brandt et al., 2008; Chu et al., 2012; Provenzale et al., 2006)) according to pathology studied are shown in Table 1, together with the median temporal resolution (not stated in three publications (Brandt et al., 2008; Chu et al., 2012; Provenzale et al., 2006)). The highest temporal resolution of 1 s was found in tumor studies (Larsson et al., 2009; Quarles et al., 2012), whereas one study on diabetes used the longest intervals, in the range of 10–30 min (Starr et al., 2003).

Vidarsson et al. (2009) and Larsson et al. (2013) investigated the influence of the temporal resolution and/or overall scan time on the quantification of BBB disruption, finding that reducing the overall scanning time and sampling with a lower temporal resolution result in increased uncertainty of the pharmacokinetic parameters K^{Trans}, v_e and v_p. As shown in Table 1, the overall scanning duration and the temporal resolution vary significantly between applications. In general, the highest temporal resolution is used in brain tumors. This is necessary to measure the fast kinetics typically seen in malignant neoplasms, but may limit spatial resolution and coverage. Conversely, studies that assess tissues with slow leakage rates (e.g. healthy appearing tissue in MS patients, aging or dementia) often use lower temporal resolutions that allow for better spatial resolution and coverage.

4.8. Use of post-processing techniques

42 of the 70 included studies (60%) did not report the use or method of image post-processing. The most commonly used technique reported was image registration, aligning the DCE-MRI images to a pre-contrast acquisition and/or anatomic images, in order to remove patient movement (Jelescu et al., 2011; Kassner et al., 2009; Wardlaw et al., 2008; Wardlaw et al., 2009; Starr et al., 2003; Starr et al., 2009; Topakian et al., 2010; Budde et al., 2012; Armitage et al., 2011; Taheri et al., 2009; Haris et al., 2008a,b,c; Aksoy et al., 2013; Lüdemann et al., 2009; Zhu et al., 2000; Ferl et al., 2010; Zhang et al., 2012; Thornhill et al., 2010; Taheri et al., 2011a; Gaitán and Shea, 2011; Shinohara et al., 2011; Larsson et al., 2013). Several studies reported a lack of precision of quantitative values due to limited spatial resolution or poor signal-to-noise ratio (Kassner et al., 2009; Ferrier et al., 2007; Cha et al., 2006; Gaitán and Shea, 2011), but only four studies report the use of image processing techniques for noise reduction, including Gaussian smoothing (Lüdemann et al., 2009), Kalman filtering (Taheri et al., 2011a,b) and unspecified smoothing of the signal enhancement curves (Ferl et al., 2010). In addition, three studies corrected DCE-MRI data for scanner signal intensity drift using phantoms. Only one study investigated the effect of scanner noise and drift on signal enhancement data (Armitage et al., 2011), concluding that studies should investigate and if necessary correct for these influences in order to prevent systematic errors.

4.9. Data analysis methods and pharmacokinetic models

A wide variety of approaches to data analysis were used in the included studies (Fig. 6). Model-free methods included the visual assessment of spatiotemporal enhancement patterns in multiple sclerosis lesions (Kermode et al., 1990; Gaitán and Shea, 2011; Shinohara et al., 2011), calculation of semi-quantitative parameters from the signal

Table 2
K^{Trans} values reported for different tissue types and pharmacokinetic models. Given values are the median [range] of reported study sample means from human (in black) and animal (in orange) studies. Please note that some subjects included in these studies (e.g. high grade glioma patients) underwent treatment before entering the study. Hence, the reported baseline parameters might be influenced by interventions that were not the focus in the study.

Pathology	K^{Trans} ($\cdot 10^{-2}$ min^{-1})			
	Conventional Tofts	Modified Tofts	Patlak	Other
Normal appearing tissue				
Mixed gray and white matter	–	0.40/1.70 [0.30 - 0.50]/[0.40 - 3.00]	0.39/0.03 [0.00 - 0.06]	0.01 [0.00 - 0.32]
White matter	–	1.60	0.20 [0.04 - 0.84]	0.04
Gray matter	–	–	0.08 [0.05 - 0.89]	–
Tumor tissue				
Mixed	6.00 [-0.37 - 25.00]	34.00	–	–
Glioma	16.60 [2.00 - 124.00]	7.95/12.60 [1.90 - 21.40]/[2.09 - 13.80]	3.10/0.97 [1.20 - 3.60]	0.70/6.25 [1.70 - 13.00]
Meningeoma	37.40 [27.80 - 47.00]	–	–	–
Astrocytoma	14.30 [2.80 - 111.00]	–	–	–
Stroke lesion				
Ischemic	–	–	0.84/0.35 [0.15 - 0.41]	1.94 [0.78 - 3.10]
Hemorrhagic	–	–	–	5.50
Multiple sclerosis lesion	2.23 [0.92 - 3.53]	–	–	0.98
Neurocysticercosis	3.50 [2.00 - 5.00]	–	–	–
Tuberculoma	242.50 [204.00 - 281.00]	–	–	–
Infective lesion	210.00	–	–	–
Traumatic injury	–	3.80 [0.19 - 4.90]	–	–

enhancement (Wardlaw et al., 2008; Wardlaw et al., 2009; Starr et al., 2003; Starr et al., 2009; Topakian et al., 2010; Brandt et al., 2008; Su et al., 1998; Miyati et al., 1997; Wang et al., 2006; Mills et al., 2009; Provenzale et al., 2006; Wilkinson et al., 2006) and/or contrast agent concentration (Budde et al., 2012; Armitage et al., 2011) curves, and model-free deconvolution (Singh et al., 2007; Larsson et al., 2009; Cramer et al., 2014; Haris et al., 2008a,c; Awasthi et al., 2012; Ferl et al., 2010; Larsen et al., 2013; Gupta et al., 2012). The most commonly used pharmacokinetic models were the conventional Tofts model (Singh et al., 2007; Jelescu et al., 2011; Li et al., 2000; Noseworthy and Bray, 2000; Haris et al., 2008a,b,c; Thompson et al., 2012; Manuchehri et al., 2007; Cha et al., 2006; Harrer et al., 2004; Zhu et al., 2000; Ferl et al., 2010; Jia et al., 2013; Gupta et al., 2012), the modified Tofts model (Li et al., 2012; Ali et al., 2010; Hoff et al., 2012; Aryal et al., 2014; Wei et al., 2011; Awasthi et al., 2012; Bagher-Ebadian et al., 2012; Cao et al., 2009; Chu et al., 2012; Harrer et al., 2004; Zhang et al., 2012; Ingrisch et al., 2012; Song et al., 2011; Larsson et al., 2013), the Patlak model (Larsson et al., 2009; Cramer et al., 2014; Abo-Ramadan et al., 2009; Durukan et al., 2009; Ewing et al., 2003; Nagaraja et al., 2010; Taheri et al., 2009; Krueck et al., 1994; Vidarsson et al., 2009; Bagher-Ebadian et al., 2012; Larsen et al., 2013; Thornhill et al., 2010; Taheri et al., 2011a,b) and a simplified approach based on the Patlak model (Kassner et al., 2009; Ferrier et al., 2007; Aksoy et al., 2013; Roberts et al., 2000; Kassner et al., 2005) as introduced by Shames et al. (1993) and Iannotti et al. (1987). Other modeling approaches included a variant of the conventional Tofts model that considers only the first pass of the contrast bolus (Li et al., 2000; Harrer et al., 2004), a two-compartment exchange (Sourbron et al., 2009; Larsson et al., 2009) and uptake (Sourbron et al., 2009; Ingrisch et al., 2012) model, and a modified two-compartment exchange model that includes two EES compartments (one in slow and one in fast exchange with the blood compartment) (Ludemann et al., 2002; Lüdemann et al., 2009; Lüdemann et al., 2000). Furthermore, one study each applied an AIF-free reference region model introduced by Yankeelov et al. (2005) in rat gliomas (Quarles et al., 2012) and a shutter-speed model considering three-site equilibrium water exchange (Li et al., 2010). Table 2 summarizes the range of K^{Trans} estimates for different tissue types and pharmacokinetic models as reported in the included publications.

Several studies aimed primarily at comparing different approaches for data analysis. Li et al. (2000) introduced a variant of the conventional Tofts model that only considers the first pass of the contrast bolus. They evaluated this method in $n = 11$ patients with primary brain neoplasms, finding that the results were visually comparable with those of the conventional Tofts model but less noisy and less susceptible to large vessel contributions. Harrer et al. (2004) evaluated the same model in $n = 18$ patients with high-grade gliomas, reporting a good correlation with the modified Tofts model but no correlation with the conventional Tofts method, though it should be noted that the AIFs used differed between the models due to software limitations. Values obtained with the conventional Tofts model were considerably higher, indicating an overestimation of quantitative parameters due to vessel contributions. Larsson et al. (2009) used simulated data in order to investigate the accuracy of the two-compartment exchange and Patlak models. As expected, they found that the Patlak method is accurate for

low values of K^{Trans}, whereas the two-compartment exchange model provides more accurate results for high K^{Trans} values (Larsson et al., 2009). Li et al. (2010) considered the effect of water exchange, finding the Patlak model to significantly underestimate the fractional blood volume when compared to their three-site equilibrium shutter-speed model. A non-parametric method for evaluating DCE-MRI in $n = 16$ glioma patients was presented by Ferl et al. (2010), who showed that their resulting parameters closely approximate the conventional Tofts model parameters. Finally, Bagher-Ebadian et al. (2012) presented a method for quantifying BBB disruption in heterogeneous glioblastoma based on a voxel-by-voxel selection from a set of nested models: the most complex model with three parameters was required to fit the data in regions of aggressive tumor growth, while simpler models predominated in less aggressive tumor portions and in healthy tissues.

5. Discussion

Our systematic review of the literature revealed 70 studies involving methods to assess BBB disruption in 15 pathologies in 417 animals and 1564 humans. These studies showed considerable heterogeneity with regard to image acquisition and analysis methods. This is partly a consequence of the wide range of tissues, pathologies and study objectives. For example, tumor studies used higher temporal resolution and shorter imaging duration on average compared with studies of less permeable tissue such as multiple sclerosis, ischemic stroke and normal appearing brain. However, it should be noted that a minority of the articles explicitly justified the methodology used. The factors influencing inter-study comparability and implications for futures studies are discussed in the following paragraphs.

5.1. Inter-study comparability of quantitative DCE-MRI parameters

Due to the wide range of analysis techniques used and their strong dependence on underlying assumptions and acquisition parameters, a lack of inter-study comparability represents a major problem. Care must be taken when comparing results from different studies as shown by the wide parameter ranges in Table 2. Some of this variability is inevitable due to the heterogeneity of the study populations (e.g. subjects' age) and study designs. Since most articles did not explicitly justify the analytical method employed, differences in the choice of pharmacokinetic model may account for some of the variation. Biased parameter estimates are likely to be obtained when the assumptions of the model are not met in the tissue or when the data acquired are inadequate to determine a unique solution. For example, several studies (e.g. Ali et al., 2010, Zhang et al., 2012) apply the same model to tumor tissue and contralateral healthy tissue, although the underlying tissue physiology is very different and one model is unlikely to be valid in both situations. The importance of appropriate model selection has been demonstrated both theoretically (Sourbron and Buckley, 2011) and experimentally in gliomas (Harrer et al., 2004) and low-permeability brain tissue (Larsson et al., 2009; Cramer and Larsson, 2014) and is discussed further in Section 5.2. Several additional factors may also influence the results of DCE-MRI studies.

Firstly, the calculation of contrast agent concentration from signal enhancement requires reliable estimation of intrinsic tissue parameters such as the pre-contrast longitudinal relaxation time $T1_0$. There are several methods of estimating $T1_0$, with variable flip angle (Brookes et al., 1999) and variable saturation time delay (Larsson et al., 1988) being the most common. The effect of uncertainty in $T1_0$ estimation on the calculation of contrast agent concentrations has been investigated by Schabel and Parker (Schabel and Parker, 2008). They demonstrate that $T1_0$ produces a significant concentration bias, which shows the importance of accounting for $T1_0$ when assessing BBB disruption in different tissue types (Armitage et al., 2011). It should also be noted that, unless T1 is measured at each time point, drifts in signal intensity may introduce further errors in pharmacokinetic parameters; as noted above, the issue of scanner stability was seldom addressed in the included articles.

Secondly, most pharmacokinetic models require the AIF to be known. Hence, determination of AIF represents a key issue in the reliable estimation of pharmacokinetic parameters. As mentioned above, there are several strategies for AIF selection and the optimal method varies according to pathology, study aims and clinical requirements (Calamante, 2013). In most applications, direct measurement of the AIF is generally considered preferable to standard or averaged AIFs (Lavini and Verhoeff, 2010). However, this method is not always possible and is susceptible to partial volume and in-flow artefacts; uncertainty remains regarding which vessel should be sampled and how, with approaches ranging from manual region of interest selection to methods for automatic vessel detection (Chen et al., 2008). There is also disagreement on whether to describe the capillary bed in terms of blood concentration or plasma concentration by correcting for the hematocrit (Hct). In the latter case, Hct should ideally be determined for every subject, but a standard value such as Hct = 0.45 is often assumed (Sourbron and Buckley, 2013). In theory, all model equations and resulting parameter values can easily be converted between conventions. However, several studies did not report this and other details, impeding reliable comparison of parameter values from different studies.

Other sources of uncertainty rarely considered in DCE-MRI studies may arise due to a lack of available data. For example, relaxivity values specific to a contrast agent, field strength and tissue/pathology are rarely known, with the consequence that uniform relaxivity across tissues and compartments is generally assumed. A further common assumption is that of fast water exchange between compartments; the influence of restricted water exchange has been described in the literature (see 100 and references therein) but models accounting for this effect have received relatively little attention.

5.2. Implications for future DCE-MRI studies of BBB disruption

Given the diversity of DCE-MRI applications in the brain, it is impossible to prescribe a universal “recipe” for future studies, though attempts have been made to better standardize methodology and reporting (Tofts et al., 1999; DCE MRI Technical Committee, 2012; Leach et al., 2012). Instead, it is essential to recognise that the optimal method is highly dependent on the specific application. An extensive body of primary DCE-MRI literature and a number of excellent review articles should help to facilitate optimal study design in the future. In the following paragraphs we discuss some of the key aspects of acquisition protocol design and data analysis. In addition to these technical aspects, it should be noted that the overall design of a study (e.g. large sample size, appropriate control group) will be particularly important given the limitations of present DCE-MRI methods. We recommend that for most applications, changes in the longitudinal relaxation rate rather than signal intensity should be measured, since the former more accurately reflects contrast agent concentration, required for quantitative pharmacokinetic analysis. A range of pulse sequences are available to obtain this data, and the optimal choice may be a compromise between speed, accuracy, spatial coverage and other factors. Two of the most critical acquisition parameters to determine are the temporal resolution and total duration of the scan, since the optimal values depend on the nature of the tissue being investigated and the quantities to be measured (Sourbron and Buckley, 2012). For example, temporal resolution of the order of a second is required to quantify tissue plasma flow; even if this quantity is of no interest, it may be necessary to account for flow in order to accurately assess permeability. The likely influence of blood flow may be determined using computer simulations, providing plausible tissue parameter ranges are available and relevant to the subjects and tissues being studied (Sourbron et al., 2009; Larsson et al., 2009). Temporal resolution must also be set against requirements for *spatial* resolution and coverage, which differ markedly between applications (e.g. focal vs. diffuse pathology). For accurate

measurement of the permeability-surface area product *PS*, the scan duration should be long enough for significant contrast extravasation to occur: this may be on the order of a few minutes in tissues such as brain tumors, but longer scans are required in less permeable tissues such as normal-appearing brain. If the EES volume fraction v_e is to be accurately measured then imaging should continue well into the "washout" phase, when the EES contrast agent concentration begins to fall. Further research is needed to investigate how variations in contrast agent types and doses affect pharmacokinetic parameters.

A wide range of pharmacokinetic models have been proposed for fitting DCE-MRI data, the most popular of which divide the tissue into well-mixed compartments. It is essential to recognize the assumptions built into these models and to assess their likely validity for a given application (Sourbron and Buckley, 2013). The original Tofts model, for example, is strictly valid only in weakly vascularized tissues, where contrast agent in the capillaries can be neglected; furthermore, the fitted K^{Trans} is equal to *PS* only when the blood flow is sufficiently high. For tissues where the vascular contribution is significant, the Patlak or extended Tofts models may be more appropriate, provided again that plasma flow is high. The choice of model should also reflect the MRI protocol: if the acquisition duration is short and BBB leakage is slow then models that do not allow back-diffusion (e.g. Patlak and tissue-uptake models) may be suitable, while application of a model that does include back-diffusion (e.g. extended Tofts model) can result in increased uncertainty in the fitted parameters. Similarly, application of a model that includes flow (e.g. tissue-uptake and two-compartment exchange models) is counterproductive if the acquired temporal resolution is insufficient. These and other considerations have been investigated theoretically by Sourbron and Buckley (2011) and are summarized accessibly in their recent review (Sourbron and Buckley, 2013). A recent investigation by Cramer et al. further emphasized the importance of appropriate model selection in the context of subtle BBB permeability (Cramer and Larsson, 2014). If it is unclear which model to select *a-priori* then data-driven approaches, e.g. use of Akaike information criteria, can be used to determine the most suitable model (Ewing and Bagher-Ebadian, 2013), although this does not guarantee that the model assumptions are met.

As most current data apply to tumors, more data are required for assessing low-level BBB abnormalities. The relative lack of methodological assessments to determine the best methods of measuring low level BBB disruption in normal or abnormal appearing brain in aging, dementia or brain microvascular disease, argue for substantially more work to determine the optimum contrast and dose, acquisition parameters, and data analysis methods.

6. Conclusion

This systematic review has highlighted the wide range of applications where DCE-MRI has been used to assess BBB integrity. We found large variations in studied pathologies, MRI procedures and data analysis methods resulting in widely varying estimates of permeability parameters. Nevertheless, DCE-MRI has been shown to provide valuable information in a growing field of applications, ranging from the grading of primary brain tumors to the assessment of healthy-appearing tissue in multiple sclerosis patients or dementia. In methodological terms, DCE-MRI is a relatively mature technique, but the lack of agreed standards for image acquisition, data modeling and study reporting hinders inter-study comparison and meta-analysis. Improved reliability of DCE-MRI, especially in subtle permeability states, is required. Where feasible, further technical development should be accompanied by attempts to establish consensus-based recommendations for data acquisition and analysis in order to improve inter-study comparability and promote wider use of DCE-MRI both clinically and in research (Tofts et al., 1999; DCE MRI Technical Committee, 2012; Leach et al., 2012).

Acknowledgments

This work was funded by the Row Fogo Charitable Trust (Ref. AD.ROW4.35), SINAPSE (Scottish Imaging Network: A Platform for Scientific Excellence - Scottish Funding Council, Ref. HR07020) and supported by NHS Lothian Research & Development.

References

Abbott, N.J., Friedman, A., 2012. Overview and introduction: the blood–brain barrier in health and disease. Epilepsia 53 (Suppl 6), 1–6. http://dx.doi.org/10.1111/j.1528-1167.2012.03696.x23134489.

Abo-Ramadan, U., Durukan, A., Pitkonen, M., Marinkovic, I., Tatlisumak, E., Pedrono, E., et al., 2009. Post-ischemic leakiness of the blood–brain barrier: a quantitative and systematic assessment by Patlak plots. Experimental Neurology 219, 328–333. http://dx.doi.org/10.1016/j.expneurol.2009.06.00219520075.

Aksoy, D., Bammer, R., Mlynash, M., Venkatasubramanian, C., Eyngorn, I., Snider, R.W., et al., 2013. Magnetic resonance imaging profile of blood–brain barrier injury in patients with acute intracerebral hemorrhage. Journal of the American Heart Association 2, e000161. http://dx.doi.org/10.1161/JAHA.113.00016123709564.

Ali, M.M., Janic, B., Babajani-Feremi, A., Varma, N.R.S., Iskander, A.S.M., Anagli, J., et al., 2010. Changes in vascular permeability and expression of different angiogenic factors following anti-angiogenic treatment in rat glioma. PLoS ONE 5, e8727. http://dx.doi.org/10.1371/journal.pone.000872720090952.

Armitage, P., Behrenbruch, C., Brady, M., Moore, N., 2005. Extracting and visualizing physiological parameters using dynamic contrast-enhanced magnetic resonance imaging of the breast. Medical Image Analysis 9, 315–329. http://dx.doi.org/10.1016/j.media.2005.01.00115950895.

Armitage, P.A., Farrall, A.J., Carpenter, T.K., Doubal, F.N., Wardlaw, J.M., 2011. Use of dynamic contrast-enhanced MRI to measure subtle blood–brain barrier abnormalities. Magnetic Resonance Imaging 29, 305–314. http://dx.doi.org/10.1016/j.mri.2010.09.00221030178.

Aryal, M.P., Nagaraja, T.N., Keenan, K.A., Bagher-Ebadian, H., Panda, S., Brown, S.L., et al., 2014. Dynamic contrast enhanced MRI parameters and tumor cellularity in a rat model of cerebral glioma at 7 T. Society of Magnetic Resonance in Medicine 71, 2206–2214. http://dx.doi.org/10.1002/mrm.2487323878070.

Awasthi, R., Pandey, C.M., Sahoo, P., Behari, S., Kumar, V., Kumar, S., et al., 2012. Dynamic contrast-enhanced magnetic resonance imaging-derived kep as a potential biomarker of matrix metalloproteinase 9 expression in patients with glioblastoma multiforme: a pilot study. Journal of Computer Assisted Tomography 36, 125–130. http://dx.doi.org/10.1097/RCT.0b013e31823f6c5922261782.

Bagher-Ebadian, H., Jain, R., Nejad-Davarani, S.P., Mikkelsen, T., Lu, M., Jiang, Q., et al., 2012. Model selection for DCE-T1 studies in glioblastoma. Magnetic Resonance in Medicine: Official Journal of the Society of Magnetic Resonance in Medicine / Society of Magnetic Resonance in Medicine 68, 241–251. http://dx.doi.org/10.1002/mrm.2321122127934.

Barnes, S.L., Whisenant, J.G., Loveless, M.E., Yankeelov, T.E., 2012. Practical dynamic contrast enhanced MRI in small animal models of cancer: data acquisition, data analysis, and interpretation. Pharmaceutics 4, 442–478. http://dx.doi.org/10.3390/pharmaceutics403044223105959.

Brandt, C.T., Simonsen, H., Liptrot, M., Søgaard, L.V., Lundgren, J.D., Ostergaard, C., et al., 2008. In vivo study of experimental pneumococcal meningitis using magnetic resonance imaging. BMC Medical Imaging 8, 1. http://dx.doi.org/10.1186/1471-2342-8-118194516.

Brix, G., Semmler, W., Port, R., 1991. Pharmacokinetic parameters in CNS Gd-DTPA enhanced MR imaging. Journal of Computer Assisted Tomography 15, 621–628. http://dx.doi.org/10.1097/00004728-199107000-000182061479.

Brookes, J.A., Redpath, T.W., Gilbert, F.J., Murray, A.D., Staff, R.T., 1999. Accuracy of T1 measurement in dynamic contrast-enhanced breast MRI using two- and three-dimensional variable flip angle fast low-angle shot. Journal of Magnetic Resonance Imaging: JMRI 9, 163–171. http://dx.doi.org/10.1002/(SICI)1522-2586(199902)9:2<163::AID-JMRI3>3.0.CO;2-L10077009.

Budde, M.D., Gold, E., Jordan, E.K., Frank, J.A., 2012. Differential microstructure and physiology of brain and bone metastases in a rat breast cancer model by diffusion and dynamic contrast enhanced MRI. Clinical & Experimental Metastasis 29, 51–62. http://dx.doi.org/10.1007/s10585-011-9428-222042553.

Calamante, F., 2013. Arterial input function in perfusion MRI: a comprehensive review. Progress in Nuclear Magnetic Resonance Spectroscopy 74, 1–32. http://dx.doi.org/10.1016/j.pnmrs.2013.04.00224083460.

Cao, Y., Tsien, C.I., Sundgren, P.C., Nagesh, V., Normolle, D., Buchtel, H., et al., 2009. Dynamic contrast-enhanced magnetic resonance imaging as a biomarker for prediction of radiation-induced neurocognitive dysfunction. Clinical Cancer Research: an Official Journal of the American Association for Cancer Research 15, 1747–1754. http://dx.doi.org/10.1158/1078-0432.CCR-08-142019223506.

Cha, S., Yang, L., Johnson, G., Lai, A., Chen, M.H., Tihan, T., et al., 2006. Comparison of microvascular permeability measurements, K Trans, determined with pass T2*-weighted MR imaging methods in gliomas and meningiomas. AJNR. American Journal of Neuroradiology 27, 409–41716484420.

Chen, J., Yao, J., Thomasson, D., 2008. Automatic determination of arterial input function for dynamic contrast enhanced MRI in tumor assessment. Medical Image Computing and Computer-Assisted Intervention: MICCAI ... International Conference on Medical Image Computing and Computer-Assisted Intervention 11, 594–60118979795.

Chu, J.-P., Mak, H.K..-F., Yau, K.K..-W., Zhang, L., Tsang, J., Chan, Q., et al., 2012. Pilot study on evaluation of any correlation between MR perfusion (Ktrans) and diffusion

(apparent diffusion coefficient) parameters in brain tumors at 3 Tesla. Cancer Imaging: the Official Publication of the International Cancer Imaging Society 12, 1–6. http://dx.doi.org/10.1102/1470-7330.2012.000122275724.
Cramer, S.P., Larsson, H.B.W., 2014. Accurate determination of blood–brain barrier permeability using dynamic contrast-enhanced T1-weighted MRI: a simulation and in vivo study on healthy subjects and multiple sclerosis patients. Journal of Cerebral Blood Flow and Metabolism: Official Journal of the International Society of Cerebral Blood Flow and Metabolism 1–11 http://dx.doi.org/10.1038/jcbfm.2014.12625074746.
Cramer, S.P., Simonsen, H., Frederiksen, J.L., Rostrup, E., Larsson, H.B.W., 2014. Abnormal blood–brain barrier permeability in normal appearing white matter in multiple sclerosis investigated by MRI. NeuroImage. Clinical 4, 182–189. http://dx.doi.org/10.1016/j.nicl.2013.12.00124371801.
DCE MRI Technical Committee, 2012. DCE MRI Quantification Profile, Quantitative Imaging Biomarkers AllianceVersion 1.0. Reviewed Draft. Available from: http://rsna.org/QIBA.aspx.
Durukan, A., Marinkovic, I., Strbian, D., Pitkonen, M., Pedrono, E., Soinne, L., et al., 2009. Post-ischemic blood–brain barrier leakage in rats: one-week follow-up by MRI. Brain Research 1280, 158–165. http://dx.doi.org/10.1016/j.brainres.2009.05.02519450568.
Ewing, J.R., Bagher-Ebadian, H., 2013. Model selection in measures of vascular parameters using dynamic contrast-enhanced MRI: experimental and clinical applications. NMR in Biomedicine 26, 1028–1041. http://dx.doi.org/10.1002/nbm.299623881857.
Ewing, J.R., Knight, R.A., Nagaraja, T.N., Yee, J.S., Nagesh, V., Whitton, P.A., et al., 2003. Patlak plots of Gd-DTPA MRI data yield blood–brain transfer constants concordant with those of 14C-sucrose in areas of blood–brain opening. Magnetic Resonance in Medicine: Official Journal of the Society of Magnetic Resonance in Medicine / Society of Magnetic Resonance in Medicine 50, 283–292. http://dx.doi.org/10.1002/mrm.1052412876704.
Ferl, G.Z., Xu, L., Friesenhahn, M., Bernstein, L.J., Barboriak, D.P., Port, R.E., 2010. An automated method for nonparametric kinetic analysis of clinical DCE-MRI data: application to glioblastoma treated with bevacizumab. Magnetic Resonance in Medicine: Official Journal of the Society of Magnetic Resonance in Medicine / Society of Magnetic Resonance in Medicine 63, 1366–1375. http://dx.doi.org/10.1002/mrm.2233520432307.
Ferrier, M.C., Sarin, H., Fung, S.H., Schatlo, B., Pluta, R.M., Gupta, S.N., et al., 2007. Validation of dynamic contrast-enhanced magnetic resonance imaging-derived vascular permeability measurements using quantitative autoradiography in the RG2 Rat brain tumor model. Neoplasia (New York, N.Y.) 9, 546–555. http://dx.doi.org/10.1593/neo.0728917710157.
Gaitán, M.I., Shea, C.D., 2011. Evolution of the blood–brain barrier in newly forming multiple sclerosis lesions. Annals of Neurology 70, 22–29. http://dx.doi.org/10.1002/ana.2247221710622.
Gal, Y., Mehnert, A., Bradley, A., McMahon, K., Kennedy, D., Crozier, S., 2008. A new denoising method for dynamic contrast-enhanced MRI. Annual International Conference of the IEEE Engineering in Medicine and Biology Society 847–850.
Gupta, R.K., Awasthi, R., Rathore, R.K.S., Verma, A., Sahoo, P., Paliwal, V.K., et al., 2012. Understanding epileptogenesis in calcified neurocysticercosis with perfusion MRI. Neurology 78, 618–625. http://dx.doi.org/10.1212/WNL.0b013e318248deae22302547.
Guyatt, G.H., Oxman, A.D., Vist, G.E., Kunz, R., Falck-Ytter, Y., Alonso-Coello, P., et al., 2008. GRADE: an emerging consensus on rating quality of evidence and strength of recommendations. BMJ (Clinical Research Ed.) 336, 924–926. http://dx.doi.org/10.1136/bmj.39489.470347.AD18436948.
Haris, M., Gupta, R.K., Singh, A., Husain, N., Husain, M., Pandey, C.M., et al., 2008a. Differentiation of infective from neoplastic brain lesions by dynamic contrast-enhanced MRI. Neuroradiology 50, 531–540. http://dx.doi.org/10.1007/s00234-008-0378-618379766.
Haris, M., Husain, N., Singh, A., Awasthi, R., Singh Rathore, R.K., Husain, M., et al., 2008b. Dynamic contrast-enhanced (DCE) derived transfer coefficient (ktrans) is a surrogate marker of matrix metalloproteinase 9 (MMP-9) expression in brain tuberculomas. Journal of Magnetic Resonance Imaging: JMRI 28, 588–597. http://dx.doi.org/10.1002/jmri.2149118777539.
Haris, M., Husain, N., Singh, A., Husain, M., Srivastava, S., Srivastava, C., et al., 2008c. Dynamic contrast-enhanced derived cerebral blood volume correlates better with Leak correction than with No correction for vascular endothelial growth factor, microvascular density, and grading of astrocytoma. Journal of Computer Assisted Tomography 32, 955–965. http://dx.doi.org/10.1097/RCT.0b013e31816200d119204461.
Harrer, J.U., Parker, G.J.M., Haroon, H.A., Buckley, D.L., Embelton, K., Roberts, C., et al., 2004. Comparative study of methods for determining vascular permeability and blood volume in human gliomas. Journal of Magnetic Resonance Imaging: JMRI 20, 748–757. http://dx.doi.org/10.1002/jmri.2018215503330.
Hoff, B.A., Bhojani, M.S., Rudge, J., Chenevert, T.L., Meyer, C.R., Galbán, S., et al., 2012. DCE and DW-MRI monitoring of vascular disruption following VEGF-Trap treatment of a rat glioma model. NMR in Biomedicine 25, 935–942. http://dx.doi.org/10.1002/nbm.181422190279.
Iannotti, F., Fieschi, C., Alfano, B., 1987. Simplified, noninvasive PET measurement of blood–brain barrier permeability. Journal of Computer Assisted Tomography 11, 390–397. http://dx.doi.org/10.1097/00004728-198705000-000043106433.
Ingrisch, M., Sourbron, S., Morhard, D., Ertl-Wagner, B., Kümpfel, T., 2012. Quantification of perfusion and permeability in multiple sclerosis: dynamic contrast-enhanced MRI in 3D at 3T. Investigative Radiology 47, 252–258. http://dx.doi.org/10.1097/RLI.0b013e31823bfc9722373532.
Jain, R., 2013. Measurements of tumor vascular leakiness using DCE in brain tumors: clinical applications. NMR in Biomedicine 26, 1042–1049. http://dx.doi.org/10.1002/nbm.299423832526.
Jelescu, I.O., Leppert, I.R., Narayanan, S., Araújo, D., Arnold, D.L., Pike, G.B., 2011. Dual-temporal resolution dynamic contrast-enhanced MRI protocol for blood–brain barrier permeability measurement in enhancing multiple sclerosis lesions. Journal of Magnetic Resonance Imaging: JMRI 33, 1291–1300. http://dx.doi.org/10.1002/jmri.2256521590997.
Jia, Z.Z., Geng, D.Y., Liu, Y., Chen, X.R., Zhang, J., 2013. Microvascular permeability of brain astrocytoma with contrast-enhanced magnetic resonance imaging: correlation analysis with histopathologic grade. Chinese Medicine J2013 (126), 1953–195623673117.
Kassner, A., Roberts, T., Taylor, K., Silver, F., Mikulis, D., 2005. Prediction of hemorrhage in acute ischemic stroke using permeability MR imaging. AJNR. American Journal of Neuroradiology 26, 2213–221716219824.
Kassner, A., Roberts, T.P.L., Moran, B., Silver, F.L., Mikulis, D.J., 2009. Recombinant tissue plasminogen activator increases blood–brain barrier disruption in acute ischemic stroke: an MR imaging permeability study. AJNR. American Journal of Neuroradiology 30, 1864–1869. http://dx.doi.org/10.3174/ajnr.A177419661169.
Kermode, A.G., Tofts, P.S., Thompson, A.J., MacManus, D.G., Rudge, P., Kendall, B.E., et al., 1990. Heterogeneity of blood–brain barrier changes in multiple sclerosis: an MRI study with gadolinium-DTPA enhancement. Neurology 40, 229–235. http://dx.doi.org/10.1212/WNL.40.2.2292300240.
Krueck, W.G., Schmiedl, U.P., Maravilla, K.R., Spence, A.M., Starr, F.L., Kenney, J., 1994. MR assessment of radiation-induced blood–brain barrier permeability changes in rat glioma model. AJNR. American Journal of Neuroradiology 15, 625–6328010261.
Larsen, V.A., Simonsen, H.J., Law, I., Larsson, H.B.W., Hansen, A.E., 2013. Evaluation of dynamic contrast-enhanced T1-weighted perfusion MRI in the differentiation of tumor recurrence from radiation necrosis. Neuroradiology 55, 361–369. http://dx.doi.org/10.1007/s00234-012-1127-423262559.
Larsson, C., Kleppestø, M., Rasmussen, I., Salo, R., Vardal, J., Brandal, P., et al., 2013. Sampling requirements in DCE-MRI based analysis of high grade gliomas: Simulations and clinical results. Journal of Magnetic Resonance Imaging: JMRI 37, 818–829. http://dx.doi.org/10.1002/jmri.2386623086710.
Larsson, H.B., Stubgaard, M., Frederiksen, J.L., Jensen, M., Henriksen, O., Paulson, O.B., 1990. Quantitation of blood–brain barrier defect by magnetic resonance imaging and gadolinium-DTPA in patients with multiple sclerosis and brain tumors. Magnetic Resonance in Medicine: Official Journal of the Society of Magnetic Resonance in Medicine / Society of Magnetic Resonance in Medicine 16, 117–131. http://dx.doi.org/10.1002/mrm.19101601112255233.
Larsson, H.B.W., Courivaud, F., Rostrup, E., Hansen, A.E., 2009. Measurement of brain perfusion, blood volume, and blood–brain barrier permeability, using dynamic contrast-enhanced T(1)-weighted MRI at 3 tesla. Magnetic Resonance in Medicine: Official Journal of the Society of Magnetic Resonance in Medicine / Society of Magnetic Resonance in Medicine 62, 1270–1281. http://dx.doi.org/10.1002/mrm.2213619780145.
Larsson, H.B.W., Frederiksen, J., Kjaer, L., Henriksen, O., Olesen, J., 1988. In vivo determination of T1 and T2 in the brain of patients with severe but stable multiple sclerosis. Magnetic Resonance in Medicine: Official Journal of the Society of Magnetic Resonance in Medicine / Society of Magnetic Resonance in Medicine 7, 43–55. http://dx.doi.org/10.1002/mrm.19100701063386521.
Lavini, C., Verhoeff, J.J.C., 2010. Reproducibility of the gadolinium concentration measurements and of the fitting parameters of the vascular input function in the superior sagittal sinus in a patient population. Magnetic Resonance Imaging 28, 1420–1430. http://dx.doi.org/10.1016/j.mri.2010.06.01720817379.
Leach, M.O., Morgan, B., Tofts, P.S., Buckley, D.L., Huang, W., Horsfield, M.A., et al., 2012. Imaging vascular function for early stage clinical trials using dynamic contrast-enhanced magnetic resonance imaging. European Radiology 22, 1451–1464. http://dx.doi.org/10.1007/s00330-012-2446-x22562143.
Li, K.-L., Buonaccorsi, G., Thompson, G., Cain, J.R., Watkins, A., Russell, D., et al., 2012. An improved coverage and spatial resolution — using dual injection dynamic contrast-enhanced (ice-DICE) MRI: a novel dynamic contrast-enhanced technique for cerebral tumors. Magnetic Resonance in Medicine: Official Journal of the Society of Magnetic Resonance in Medicine / Society of Magnetic Resonance in Medicine 68, 452–462. http://dx.doi.org/10.1002/mrm.2325222791559.
Li, K.L., Zhu, X.P., Waterton, J., Jackson, A., 2000. Improved 3D quantitative mapping of blood volume and endothelial permeability in brain tumors. Journal of Magnetic Resonance Imaging: JMRI 12, 347–357. http://dx.doi.org/10.1002/1522-2586(200008)12:2<347::AID-JMRI19>3.3.CO;2-Z10931600.
Li, X., Rooney, W.D., Várallyay, C.G., Gahramanov, S., Muldoon, L.L., Goodman, J.A., et al., 2010. Dynamic-contrast-enhanced-MRI with extravasating contrast reagent: Rat cerebral glioma blood volume determination. Journal of Magnetic Resonance (San Diego, Calif.: 1997) 206, 190–199. http://dx.doi.org/10.1016/j.jmr.2010.07.00420674422.
Lüdemann, L., Hamm, B., Zimmer, C., 2000. Pharmacokinetic analysis of glioma compartments with dynamic Gd-DTPA-enhanced magnetic resonance imaging. Magnetic Resonance Imaging 18, 1201–1214. http://dx.doi.org/10.1016/S0730-725X(00)00223-X11167040.
Lüdemann, L., Warmuth, C., Plotkin, M., Förschler, A., Gutberlet, M., Wust, P., et al., 2009. Brain tumor perfusion: comparison of dynamic contrast enhanced magnetic resonance imaging using T1, T2, and T2* contrast, pulsed arterial spin labeling, and H2(15)O positron emission tomography. European Journal of Radiology 70, 465–474. http://dx.doi.org/10.1016/j.ejrad.2008.02.01218359598.
Ludemann, L., Wurm, R., Zimmer, C., 2002. Pharmacokinetic modeling of Gd-DTPA extravasation in brain tumors. Investigative Radiology 37, 562–570. http://dx.doi.org/10.1097/00004424-200210000-0000512352165.
Manuchehri, A.M., Sathyapalan, T., Lowry, M., Turnbull, L.W., Rowland-Hill, C., Atkin, S.L., 2007. Effect of dopamine agonists on prolactinomas and normal pituitary assessed by dynamic contrast enhanced magnetic resonance imaging (DCE-MRI). Pituitary 10, 261–266. http://dx.doi.org/10.1007/s11102-007-0048-417557207.

Mills, S.J., Soh, C., O'Connor, J.P.B., Rose, C.J., Buonaccorsi, G.A., Cheung, S., et al., 2009. Tumour enhancing fraction (EnF) in glioma: relationship to tumour grade. European Radiology 19, 1489–1498. http://dx.doi.org/10.1007/s00330-008-1288-z19198847.

Miyati, T., Banno, T., Mase, M., Kasai, H., Shundo, H., Imazawa, M., et al., 1997. Dual dynamic contrast-enhanced MR imaging. Journal of Magnetic Resonance Imaging: JMRI 7, 230–235. http://dx.doi.org/10.1002/jmri.18800701369039621.

Nagaraja, T.N., Karki, K., Ewing, J.R., Divine, G.W., Fenstermacher, D., Patlak, C.S., et al., 2010. The MRI-measured arterial input function resulting from a bolus injection of Gd-DTPA in a rat model of stroke slightly underestimates that of Gd-[14C]DTPA and marginally overestimates the blood-to-brain influx rate constant determined by Patlak plots. Magnetic Resonance Imaging 63, 1502–1509.

Noseworthy, M.D., Bray, T.M., 2000. Zinc deficiency exacerbates loss in blood–brain barrier integrity induced by hyperoxia measured by dynamic MRI. Proceedings of the Society for Experimental Biology and Medicine. Society for Experimental Biology and Medicine (New York, N.Y.) 223, 175–182. http://dx.doi.org/10.1111/j.1525-1373.2000.22324.x10654621.

O'Connor, J.P.B., Jackson, A., Parker, G.J.M., Roberts, C., Jayson, G.C., 2012. Dynamic contrast-enhanced MRI in clinical trials of antivascular therapies. Nature Reviews. Clinical Oncology 9, 167–177. http://dx.doi.org/10.1038/nrclinonc.2012.222330689.

Obermeier, B., Daneman, R., Ransohoff, R.M., 2013. Development, maintenance and disruption of the blood–brain barrier. Nature Medicine 19, 1584–1596. http://dx.doi.org/10.1038/nm.340724309662.

Parker, G.J.M., Roberts, C., Macdonald, A., Buonaccorsi, G.A., Cheung, S., Buckley, D.L., et al., 2006. Experimentally-derived functional form for a population-averaged high-temporal-resolution arterial input function for dynamic contrast-enhanced MRI. Magnetic Resonance in Medicine: Official Journal of the Society of Magnetic Resonance in Medicine / Society of Magnetic Resonance in Medicine 56, 993–1000. http://dx.doi.org/10.1002/mrm.2106617036301.

Provenzale, J.M., York, G., Moya, M.G., Parks, L., Choma, M., Kealey, S., et al., 2006. Correlation of relative permeability and relative cerebral blood volume in high-grade cerebral neoplasms. AJR. American Journal of Roentgenology 187, 1036–1042. http://dx.doi.org/10.2214/AJR.04.067616985154.

Quarles, C.C., Gore, J.C., Xu, L., Yankeelov, T.E., 2012. Comparison of dual-echo DSC-MRI- and DCE-MRI-derived contrast agent kinetic parameters. Magnetic Resonance Imaging 30, 944–953. http://dx.doi.org/10.1016/j.mri.2012.03.00822617148.

Roberts, H.C., Roberts, T.P., Brasch, R.C., Dillon, W.P., 2000. Quantitative measurement of microvascular permeability in human brain tumors achieved using dynamic contrast-enhanced MR imaging: correlation with histologic grade. AJNR. American Journal of Neuroradiology 21, 891–89910815665.

Rosenberg, G.A., 2012. Neurological diseases in relation to the blood–brain barrier. Journal of Cerebral Blood Flow and Metabolism: Official Journal of the International Society of Cerebral Blood Flow and Metabolism 32, 1139–1151. http://dx.doi.org/10.1038/jcbfm.2011.19722252235.

Schabel, M.C., Parker, D.L., 2008. Uncertainty and bias in contrast concentration measurements using spoiled gradient echo pulse sequences. Physics in Medicine and Biology 53, 2345–2373. http://dx.doi.org/10.1088/0031-9155/53/9/01018421121.

Shames, D.M., Kuwatsuru, R., Vexler, V., Mühler, A., Brasch, R.C., 1993. Measurement of capillary permeability to macromolecules by dynamic magnetic resonance imaging: a quantitative noninvasive technique. Magnetic Resonance in Medicine: Official Journal of the Society of Magnetic Resonance in Medicine / Society of Magnetic Resonance in Medicine 29, 616–622. http://dx.doi.org/10.1002/mrm.19102905068505897.

Shinohara, R.T., Crainiceanu, C.M., Caffo, B.S., 2011. Population-wide principal component-based quantification of blood–brain-barrier dynamics in multiple sclerosis. Neuroimage 57, 1430–1446. http://dx.doi.org/10.1016/j.neuroimage.2011.05.03821635955.

Singh, A., Haris, M., Rathore, D., Purwar, A., Sarma, M., Bayu, G., et al., 2007. Quantification of physiological and hemodynamic indices using T(1) dynamic contrast-enhanced MRI in intracranial mass lesions. Journal of Magnetic Resonance Imaging: JMRI 26, 871–880. http://dx.doi.org/10.1002/jmri.2108017896358.

Song, S.K., Lee, S.-K., Lee, J.J., Lee, J.E., Choi, H.S., Sohn, Y.H., et al., 2011. Blood–brain barrier impairment is functionally correlated with clinical severity in patients of multiple system atrophy. Neurobiology of Aging 32, 2183–2189. http://dx.doi.org/10.1016/j.neurobiolaging.2009.12.01720149484.

Sourbron, S., Ingrisch, M., Siefert, A., Reiser, M., Herrmann, K., 2009. Quantification of cerebral blood flow, cerebral blood volume, and blood–brain-barrier leakage with DCE-MRI. Magnetic Resonance in Medicine: Official Journal of the Society of Magnetic Resonance in Medicine / Society of Magnetic Resonance in Medicine 62, 205–217. http://dx.doi.org/10.1002/mrm.2200519449435.

Sourbron, S.P., Buckley, D.L., 2013. Classic models for dynamic contrast-enhanced MRI. NMR in Biomedicine 26, 1004–1027. http://dx.doi.org/10.1002/nbm.294023674304.

Sourbron, S.P., Buckley, D.L., 2011. On the scope and interpretation of the Tofts models for DCE-MRI. Magnetic Resonance in Medicine: Official Journal of the Society of Magnetic Resonance in Medicine / Society of Magnetic Resonance in Medicine 66, 735–745. http://dx.doi.org/10.1002/mrm.2286121384424.

Sourbron, S.P., Buckley, D.L., 2012. Tracer kinetic modelling in MRI: estimating perfusion and capillary permeability. Physics in Medicine and Biology 57, R1–33. http://dx.doi.org/10.1088/0031-9155/57/2/R122173205.

Starr, J.M., Farrall, A.J., Armitage, P., McGurn, B., Wardlaw, J., 2009. Blood–brain barrier permeability in Alzheimer's disease: A case-control MRI study. Psychiatry Research 171, 232–241. http://dx.doi.org/10.1016/j.pscychresns.2008.04.00319211227.

Starr, J.M., Wardlaw, J., Ferguson, K., MacLullich, A., Deary, I.J., Marshall, I., 2003. Increased blood–brain barrier permeability in type II diabetes demonstrated by gadolinium magnetic resonance imaging. Journal of Neurology, Neurosurgery, and Psychiatry 74, 70–76. http://dx.doi.org/10.1136/jnnp.74.1.7012486269.

Su, M.Y., Head, E., Brooks, W.M., Wang, Z., Muggenburg, B.A., Adam, G.E., et al., 1998. Magnetic resonance imaging of anatomic and vascular characteristics in a canine model of human aging. Neurobiology of Aging 19, 479–485. http://dx.doi.org/10.1016/S0197-4580(98)00081-59880050.

Taheri, S., Candelario-Jalil, E., Estrada, E.Y., Rosenberg, G.A., 2009. Spatiotemporal correlations between blood–brain barrier permeability and apparent diffusion coefficient in a rat model of ischemic stroke. PloS One 4, e6597. http://dx.doi.org/10.1371/journal.pone.000659719668371.

Taheri, S., Gasparovic, C., Huisa, B.N., Adair, J.C., Edmonds, E., Prestopnik, J., et al., 2011a. Blood–brain barrier permeability abnormalities in vascular cognitive impairment. Stroke; a Journal of Cerebral Circulation 42, 2158–2163. http://dx.doi.org/10.1161/STROKEAHA.110.61173121719768.

Taheri, S., Gasparovic, C., Shah, N.J., Rosenberg, G.A., 2011b. Quantitative measurement of blood–brain barrier permeability in human using dynamic contrast-enhanced MRI with fast T1 mapping. Magnetic Resonance in Medicine: Official Journal of the Society of Magnetic Resonance in Medicine / Society of Magnetic Resonance in Medicine 65, 1036–1042. http://dx.doi.org/10.1002/mrm.2268621413067.

Thompson, E.M., Guillaume, D.J., Dósa, E., Li, X., Nazemi, K.J., Gahramanov, S., et al., 2012. Dual contrast perfusion MRI in a single imaging session for assessment of pediatric brain tumors. Journal of Neuro-Oncology 109, 105–114. http://dx.doi.org/10.1007/s11060-012-0872-x22528798.

Thornhill, R.E., Chen, S., Rammo, W., Mikulis, D.J., Kassner, A., 2010. Contrast-enhanced MR imaging in acute ischemic stroke: T2* measures of blood–brain barrier permeability and their relationship to T1 estimates and hemorrhagic transformation. AJNR. American Journal of Neuroradiology 31, 1015–1022. http://dx.doi.org/10.3174/ajnr.A200320190209.

Tofts, P.S., Brix, G., Buckley, D.L., Evelhoch, J.L., Henderson, E., Knopp, M.V., et al., 1999. Contrast-enhanced T 1 -Weighted MRI of a diffusible tracer: Standardized quantities and symbols. Journal of Magnetic Resonance Imaging 232, 223–232.

Tofts, P.S., Kermode, A.G., 1991. Measurement of the blood–brain barrier permeability and leakage space using dynamic MR imaging. 1. Fundamental concepts. Magnetic Resonance in Medicine: Official Journal of the Society of Magnetic Resonance in Medicine / Society of Magnetic Resonance in Medicine 17, 357–367. http://dx.doi.org/10.1002/mrm.19101702082062210.

Topakian, R., Barrick, T.R., Howe, F.A., Markus, H.S., 2010. Blood–brain barrier permeability is increased in normal-appearing white matter in patients with lacunar stroke and leucoaraiosis. Journal of Neurology, Neurosurgery, and Psychiatry 81, 192–197. http://dx.doi.org/10.1136/jnnp.2009.17207219710048.

Türkbey, B., Thomasson, D., Pang, Y., Bernardo, M., Choyke, P.L., 2010. The role of dynamic contrast-enhanced MRI in cancer diagnosis and treatment. Diagnostic and Interventional Radiology (Ankara, Turkey) 16, 186–192. http://dx.doi.org/10.4261/1305-3825.DIR.2537-08.119885783.

Vidarsson, L., Thornhill, R.E., Liu, F., Mikulis, D.J., Kassner, A., 2009. Quantitative permeability magnetic resonance imaging in acute ischemic stroke: how long do we need to scan? Magnetic Resonance Imaging 27, 1216–1222. http://dx.doi.org/10.1016/j.mri.2009.01.01919695816.

Wang, H., Golob, E.J., Su, M.-Y., 2006. Vascular volume and blood–brain barrier permeability measured by dynamic contrast enhanced MRI in hippocampus and cerebellum of patients with MCI and normal controls. Journal of Magnetic Resonance Imaging: JMRI 24, 695–700. http://dx.doi.org/10.1002/jmri.2066916878309.

Wardlaw, J.M., Doubal, F., Armitage, P., Chappell, F., Carpenter, T., Muñoz Maniega, S., et al., 2009. Lacunar stroke is associated with diffuse blood–brain barrier dysfunction. Annals of Neurology 65, 194–202. http://dx.doi.org/10.1002/ana.2154919260033.

Wardlaw, J.M., Farrall, A., Armitage, P.A., Carpenter, T., Chappell, F., Doubal, F., et al., 2008. Changes in background blood–brain barrier integrity between lacunar and cortical ischemic stroke subtypes. Stroke; a Journal of Cerebral Circulation 39, 1327–1332. http://dx.doi.org/10.1161/STROKEAHA.107.50012418309161.

Wei, X.-E., Wang, D., Li, M.-H., Zhang, Y.-Z., Li, Y.-H., Li, W.-B., 2011. A useful tool for the initial assessment of blood–brain barrier permeability after traumatic brain injury in rabbits: dynamic contrast-enhanced magnetic resonance imaging. Journal of Trauma 71, 1645–1650. http://dx.doi.org/10.1097/TA.0b013e31823498eb22182873.

Weinmann, H.J., Laniado, M., Mützel, W., 1984. Pharmacokinetics of GdDTPA/dimeglumine after intravenous injection into healthy volunteers. Physiological Chemistry and Physics and Medical NMR 16, 167–1726505043.

Wilkinson, I.D., Jellineck, D.A., Levy, D., Giesel, F.L., Romanowski, C.A.J., Miller, B.-A., et al., 2006. Dexamethasone and enhancing solitary cerebral mass lesions: alterations in perfusion and blood–tumor barrier kinetics shown by magnetic resonance imaging. Neurosurgery 58, 640–646. http://dx.doi.org/10.1227/01.NEU.0000204873.68395.A016575327.

Yankeelov, T.E., Luci, J.J., Lepage, M., Li, R., Debusk, L., Lin, P.C., et al., 2005. Quantitative pharmacokinetic analysis of DCE-MRI data without an arterial input function: a reference region model. Magnetic Resonance Imaging 23, 519–529. http://dx.doi.org/10.1016/j.mri.2005.02.01315919597.

Zhang, N., Zhang, L., Qiu, B., Meng, L., Wang, X., Hou, B.L., 2012. Correlation of volume transfer coefficient Ktrans with histopathologic grades of gliomas. Journal of Magnetic Resonance Imaging: JMRI 36, 355–363. http://dx.doi.org/10.1002/jmri.2367522581762.

Zhu, X.P., Li, K.L., Kamaly-Asl, I.D., Checkley, D.R., Tessier, J.J., Waterton, J.C., et al., 2000. Quantification of endothelial permeability, leakage space, and blood volume in brain tumors using combined T1 and T2* contrast-enhanced dynamic MR imaging. Journal of Magnetic Resonance Imaging: JMRI 11, 575–585. http://dx.doi.org/10.1002/1522-2586(200006)11:6<575::AID-JMRI2>3.0.CO;2-110862055.